CERN-TH-2022-212

PROCEEDINGS OF SCIENCE

LapH interpolating fields with open boundary conditions

Michele Della Morte,[a] **Olmo Francesconi**[a,*] **and Justus Tobias Tsang**[b]

[a] *CP3-Origins and IMADA, University of Southern Denmark, Campusvej 55, 5230 Odense M, Denmark*
[b] *Theoretical Physics Department, CERN, 1211 Geneva 23, Switzerland*

E-mail: francesconi@imada.sdu.dk

The stochastic Laplacian Heaviside (LapH) method has proven to be successful in hadronic calculations. In this work, with charm–light spectroscopy in mind, we set up and optimise the LapH procedure limiting ourselves to the evaluation of two–point mesonic correlation functions. The calculations are performed on CLS ensembles with $N_f = 2 + 1$ Wilson-Clover fermions on a $32^3 \times 64$ lattice with open boundary conditions. We analyse the interplay between the LapH parameters and the boundary effects, and implement a fitting procedure to isolate excitations coming from the border.

The 39th International Symposium on Lattice Field Theory,
8th-13th August, 2022,
Rheinische Friedrich-Wilhelms-Universität Bonn, Bonn, Germany

*Speaker

PoS(LATTICE2022)260

1. Introduction

In this work, we analyse the behaviour of the Laplacian-Heaviside (LapH) [1] smearing procedure in the presence of open boundary conditions. By evaluating the pseudoscalar meson two–point functions we determine the portion of the lattice unaffected by the boundary and the optimal LapH setup.

Our aim is the study of semileptonic decays in this framework, a largely unexplored setup [2]. The evaluation of three–point functions with local current insertions gives access to various quantities relevant to flavour physics. The combination of theory predictions of semileptonic form factors with experimental data gives access to components of the Cabibbo-Kobayashi-Maskawa (CKM) matrix [3, 4], where an increase in precision could lead to hints of new physics. Also, the present tension in lepton flavour universality [5] makes the study of semileptonic processes particularly interesting.

One source of uncertainty which limits the attainable precision of current theory predictions arises from the trade-off between the contamination due to excited states in the two– and three–point functions and the increased statistical uncertainty when their separation increases. Short separations between source and sink make the evaluation of plateau in the relevant quantities a delicate task and typically require sophisticated fitting procedures. The LapH smearing procedure ameliorates the effects of excited states on the relevant correlation functions.

Ensembles with open boundary conditions pave the path towards finer lattice spacings, which are particularly relevant for heavy–light flavour phenomenology. However, this requires to control any effects that might arise from the open boundaries, which we aim to explore in this work.

2. Computation of meson two–point functions

Our computations are based on the recently developed LapH [1] smearing procedure implemented on each time–slice by the smearing matrix

$$\mathcal{S}(\bar{x},\bar{y}) = \Theta\left(\sigma_s^2 + \Delta\right) \simeq V_s V_s^\dagger, \tag{1}$$

where V_s is the matrix containing columns of the eigenvectors associated with the N_{ev} lowest-lying eigenvalues of the 3D Laplacian Δ. The smeared quark fields thus take the form

$$\tilde{\chi} = \chi\mathcal{S} = \bar{\psi}\gamma_4\mathcal{S}, \qquad \tilde{\psi} = \mathcal{S}\psi. \tag{2}$$

Then, by introducing some $Z(N)$ noise vectors ρ in the LapH eigenspace and by defining the related dilution projector $\mathcal{P}$ in the time, spin and ev space [6] one can identify two new objects: quark sinks $\varphi = \mathcal{S}\Omega^{-1}V_s\mathcal{P}\rho$ and quark sources $\varrho = V_s\mathcal{P}\rho$, where only the former requires a Dirac matrix inversion to be computed. With these building blocks, the meson correlation functions take the form

$$C(t-t_0) = \langle \tilde{\chi}_a(t)\Gamma^A\tilde{\psi}_a(t)\ \tilde{\chi}_b(t_0)\Gamma^B\tilde{\psi}_b(t_0)\rangle = \langle \Gamma^B\, Q_{ba}(t_0,t)\, \Gamma^A\, Q_{ab}(t,t_0)\rangle \tag{3}$$

$$= \langle \Gamma^B\varphi_b(t_0)\varrho_a(t)^*\Gamma^A\varphi_a(t)\varrho_b(t_0)^*\rangle = \langle \Gamma^B\bar{\varrho}_b(t_0)\bar{\varphi}_a(t)^*\Gamma^A\varphi_a(t)\varrho_b(t_0)^*\rangle \tag{4}$$

$$= \langle \mathcal{M}^{\Gamma^A}(\bar{\varphi},\varphi,t)\ \mathcal{M}^{\Gamma^B}(\bar{\varrho},\varrho,t_0)^*\rangle. \tag{5}$$

id	a[fm]	N_s	N_t	κ_l	κ_s	κ_c [9]	m_π[MeV]	m_K[MeV]
$B105$	0.086	32	64	0.136970	0.13634079	0.123244(19)	280	480

Table 1: Relevant parameters for the lattice ensemble studied in this work.

Where $\mathcal{M}$ are the (LapH subspace-sized) diluted meson fields. In this work we are interested only in evaluating pseudoscalar mesons, therefore we will study only the $A_{1u}^{(+)}$ channel of the octahedral symmetry group. Moreover, we are going to employ a trivial $Z(1)$ noise vector, and no dilution scheme, therefore restricting ourselves to *exact distillation*.

Due to the open boundary conditions, and up to leading order in chiral perturbation theory, we expect the two–point functions to fall off as [7]

$$C(t) \propto \sinh\big(m(\tilde{T} - t)\big), \tag{6}$$

where $\tilde{T}$ is a free parameter. In particular, it defines a "virtual" lattice border inside the lattice itself and can be easily obtained via a fit.

3. Results

Measurements are performed on configurations generated by the CLS initiative [8] with $N_f = 2+1$ non-perturbatively improved Wilson fermions with open boundary conditions, details of which are given in Table 1. Gauge averages are extracted from a subsample of 100 configurations and error estimates are obtained from the bootstrap procedure. On each configuration, we generate the LapH subspace with 96 eigenvectors from which we compute the pseudoscalar meson fields at three source positions $t_0 = 9, 15, 31$. Since we are using exact distillation, the meson correlation functions with fewer numbers of eigenvectors can be obtained without any additional computations by considering the $4N_{ev} \times 4N_{ev}$ square sub-matrix for each of the meson field matrices.

3.1 Boundary effect on the LapH eigenspace

As a first step to estimate the effect of the open boundary conditions on the LapH subspace we consider the gauge average the LapH eigenvalues as a function of the lattice time coordinate. Periodic boundary conditions guarantee translational invariance of the LapH subspace, while with open boundary conditions this might not be the case. As can be seen from the left–hand panel of figure 1, we observe that the eigenvalues are time–independent provided they are sufficiently far from the boundary. For the ensemble under consideration this amounts to approximately 12 time–slices ($\sim$ 1 fm). Taking the bulk value to be the average of the central 24 time–slices, the right–hand panel of the same figure shows the relative deviation from this for each eigenvalue. We find that the deviation from the bulk value is to a good approximation exponential.

3.2 Considerations on the realness of the meson correlation function

Another important aspect of the computation of the two–point functions with open boundary conditions concerns the effects that boundary vacuum states have on the correlation function. Following [10] where the analogous discussion for the Schrödinger functional case is presented, we

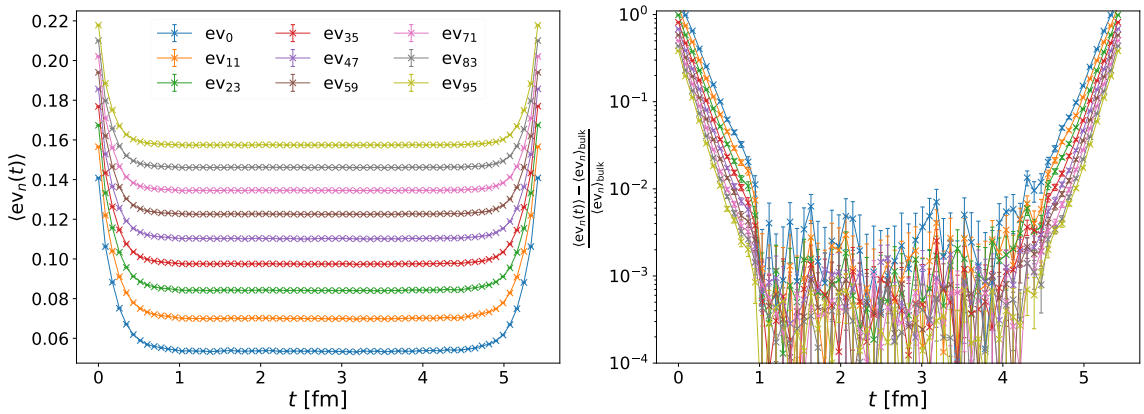

Figure 1: Left: eigenvalues of the Laplacian as a function of the lattice time coordinate. **Right**: deviation from the bulk value for each eigenvalue.

write a two–point function with open boundary conditions in the quantum mechanical representation as

$$C_2(t_1, t_2) = \frac{1}{Z}\langle i_0|P(t_1)P^\dagger(t_2)|i_0\rangle \ , \quad t_1 > t_2 \ , \tag{7}$$

where $|i_0\rangle$ is the state at the boundaries, with vacuum quantum numbers. In general

$$|i_0\rangle = w_0|0\rangle + w_1|0'\rangle + \cdots \tag{8}$$

where $|0\rangle$ is the lowest eigenstate of the Hamiltonian H and $|0'\rangle$ is the first excited vacuum state. Note that in this formulation the overlap factors w_i are in general complex and the partition function reads $\langle i_0|e^{-TH}|i_0\rangle$, where T is the temporal extent of the lattice. Now, up to a constant, the two–point function in the Heisenberg picture is

$$C_2(t_1, t_2) \propto \langle i_0|e^{-(T-t_1)H}Pe^{-(t_1-t_2)H}P^\dagger e^{-t_2 H}|i_0\rangle \ . \tag{9}$$

We consider the different contributions starting with the vacuum-vacuum contribution to $C_2(t_1, t_2)$

$$w_0^* w_0 \langle 0|Pe^{-(t_1-t_2)H}P^\dagger|0\rangle \ , \tag{10}$$

which, under the assumptions above, is real. In order to simplify the discussion we assume that P excites just one state out of $|0\rangle$ and a different one out of $|0'\rangle$. The two ground state vacuum to first excited state vacuum contributions read

$$w_0 w_1^* \langle 0'|e^{-(T-t_1)E_{0'}}Pe^{-(t_1-t_2)H}P^\dagger|0\rangle \ , \text{ and } \quad w_0^* w_1 \langle 0|Pe^{-(t_1-t_2)H}P^\dagger e^{-E_{0'}t_2}|0'\rangle \ . \tag{11}$$

Even within the strong assumptions above their sum is not real.

However, as long as only pure QCD is taken into account, a single meson state can be represented equivalently with the two charge conjugated flavour combinations, and the resulting correlation functions are complex conjugates of each other. If the boundary contaminations are small, the real part of the correlation functions still correctly represents the meson state.

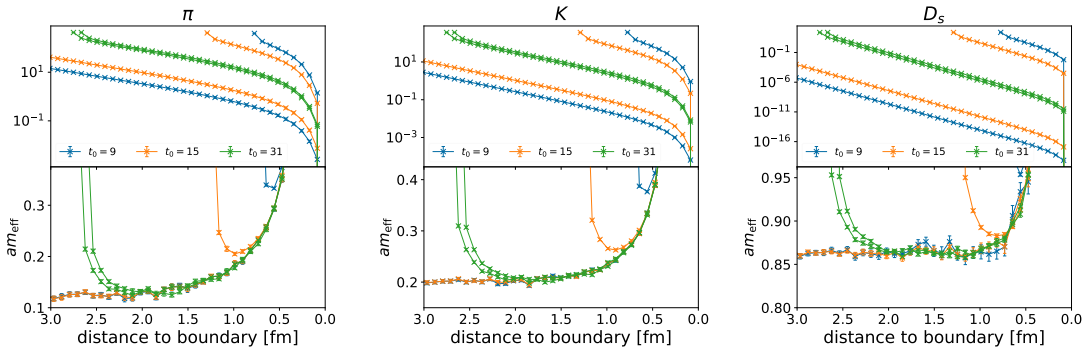

Figure 2: Comparison of meson correlation functions for the pion (left), kaon (middle) and the D_s (right) computed at source times $t_0 = 9, 15, 31$ and with $N_{ev} = 96$. The top panels show the correlation functions, the bottom panels the effective mass.

3.3 Boundary effects on the meson correlation functions

Now we consider the results for the two–point functions computed with the machinery described above. In the following we restrict ourselves to the evaluation of the correlation functions for π, K and D_s pseudoscalar mesons, and the corresponding effective masses computed as $m(t + 1/2) = \log(C(t)/C(t+1))$. To ensure that we have full control over all contributions to the correlation function, we want to understand and disentangle the effects arising from the LapH parameters and those coming from the boundaries.

In figure 2 we plot the two–point functions as a function of the distance from the nearest boundary. The boundary effects are clearly visible at the right hand edges of the various panels. The fact that the different branches all coincide close to the boundary shows that these effects are independent of the source position. They correspond to a tower of excitations arising from the boundary. In the cases where sufficiently many time slices are available and at this level of statistical uncertainty, we observe the onset of a plateau at $\sim 2.0, 1.8, 1.0$ fm from the boundary for π, K and D_s, respectively.

In figure 3 we restrict ourselves to a single source position $t_0 = 15$ and investigate how quickly the effective mass approaches the plateau as a function of the number of eigenvectors used in the construction of the LapH subspace. As expected, a smaller number of lowest-lying eigenvectors results in a broader smearing and less contamination by excited states near the source. We observe a moderate increase in the statistical uncertainty as the number of eigenvectors is reduced. In our setup we estimate the optimal number of eigenvalues to be around 24.

Lastly, in figure 4 we show the forward–time correlation functions for $N_{ev} = 24$ and compare the short time–separation behaviour for three source positions. The asymptotic value to which the effective mass approaches is compatible with the literature [8] (for the case of π and K) or in good agreement with the physical value (for the D_s). However, for the case of the pion and kaon at small time separations from the source, we observe that the $t_0 = 9$ data set deviates from the other two source positions. Crucially, this contamination does not arise from the farther boundary, but rather from the one close to the source. We conclude that this amounts to a mixing between the excited states generated at the source and those generated at the boundary.

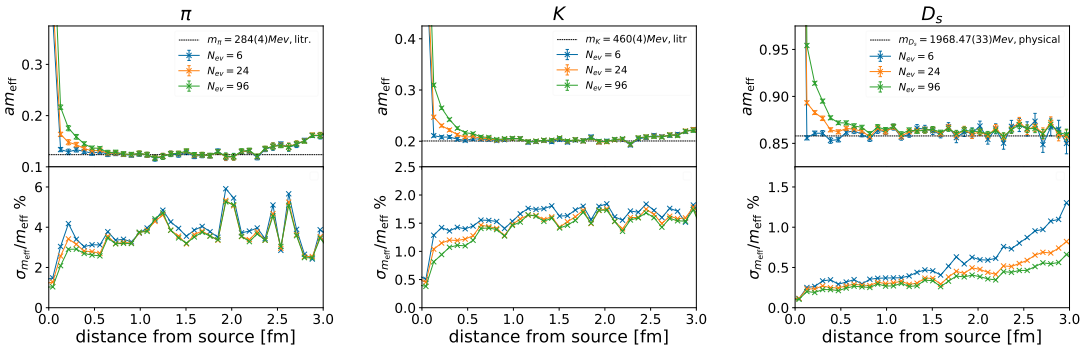

Figure 3: Comparison of the meson effective masses (top) and the relative uncertainties (bottom) for varying number of eigenvectors $N_{ev} = 6, 24, 96$. The correlation functions are computed for one fixed source at $t_0 = 15$ and we restrict ourselves to the forward branch.

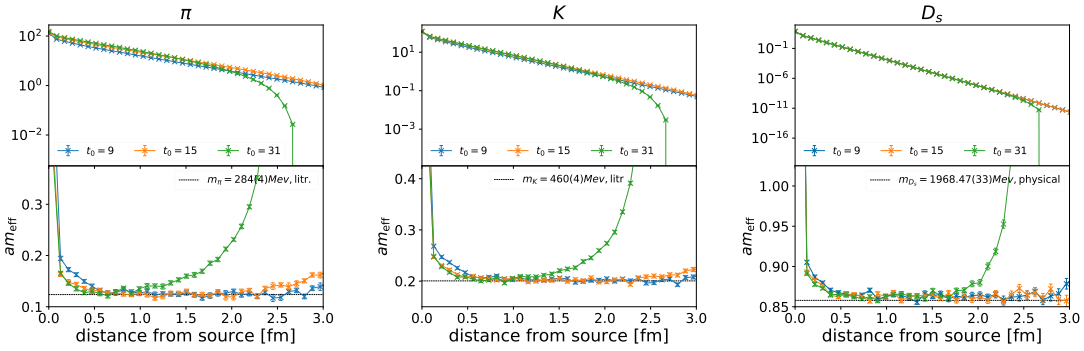

Figure 4: Comparison of the forward branch of the meson correlation functions (top) and effective masses (bottom) computed at different source times $t_0 = 9, 15, 31$ and with $N_{ev} = 24$.

However, as shown in figure 2, the boundary effects are a global characteristic of the lattice to which we have access by considering the large time separation behaviour of the meson correlation functions. In particular, the correlation functions are well described by eq. 6 and the parameters m and $\tilde{T}$ can be determined from a fit. Subsequently, we can define a continuous estimate of the effective mass of the meson state as

$$m_{\rm sinh}(t) \equiv \frac{\rm d}{{\rm d}t} \log\left(\sinh\big(m(\tilde{T}-t)\big)\right) = m\ \coth\big(m(\tilde{T}-t)\big). \tag{12}$$

We define the correction term $m_{\rm corr}$ by subtracting the fitted meson mass m from the quantity $m_{\rm sinh}(t)$, i.e.

$$m_{\rm corr}(t) = m_{\rm sinh}(t) - m. \tag{13}$$

This quantifies the amount of contamination stemming from the presence of the open boundary conditions. Since we are interested into the corrections coming from both open boundaries we correct our numerical estimate for the effective mass ($m_{\log}(t)$) with $m_{\rm corr}$ and its time reverse

$$m_{\rm eff}(t) = m_{\log}(t) - m_{\rm corr}(t) - m_{\rm corr}(T-t). \tag{14}$$

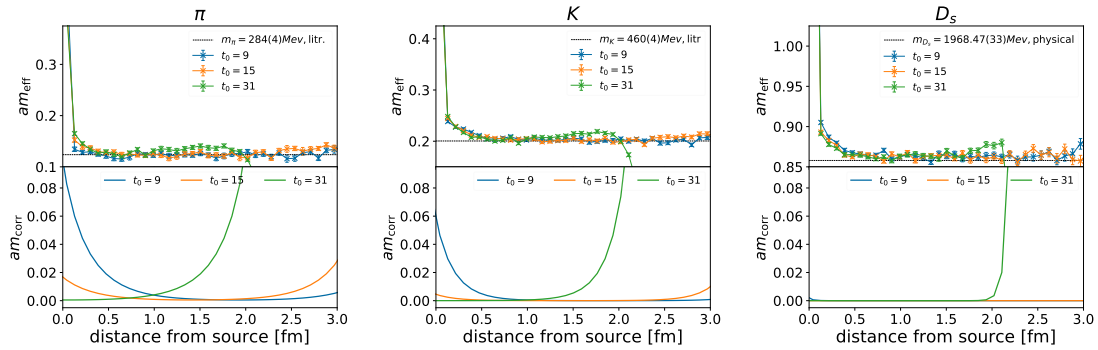

Figure 5: Comparison of the corrected effective masses (top) for π, K and D_s respectively, and the corresponding cumulative correction $m_{\rm corr}(t) + m_{\rm corr}(T-t)$ (bottom).

As shown in figure 5, this procedure is able to substantially reduce the boundary effects on the effective masses. For each meson, we extracted the two parameters $\tilde{T}$ and m by simultaneously fitting the two longer branches of the meson correlation functions generated from the sources at $t_0 = 9$ and 15. In all cases we obtain values of the reduced χ^2 lower that unity. While some deviations are still visible close to $\tilde{T}$, the corrected effective masses show clear plateaux for a wide range of time separations. This fitting procedure can be easily adapted to the evaluation of the ratios of two– and three–point correlation functions required for the study of semileptonic decays.

4. Conclusions and future developments

We have performed an extensive analysis of the effects of open boundary conditions on the two–point correlation function computed with the LapH formalism. On the ensemble we analysed and for our given statistical uncertainties, we found that the region affected by the boundary extends into the lattice for 1 fm (12 time–slices), leaving us with more than half of the lattice where the time translational invariance is restored. Our two–point functions analysis lead to the identification of an optimal setup fixing the source position at $t_0 \sim 15$ and number of eigenvectors to $N_{ev} \sim 24$.

We further devised a fitting procedure that allows for the estimate of the boundary contribution to the effective masses and a possible correction scheme that has proven to greatly reduce the boundary effects on the meson effective masses and that is largely independent of the source/sink positions.

Moreover, we have started generating data for three–point functions with local current insertions. Using to the distillation workflow this will allow for the evaluation of the processes needed to study CKM matrix elements and semileptonic form factors with minimal computational overhead.

5. Acknowledgments

The work of J.T.T. has received funding from the European Union's Horizon 2020 research and innovation programme under the Marie Skłodowska-Curie grant agreement No 894103. The DFF Research project 1. Grant n. 8021-00122B fully supports the work of O.F. and partially supports M.D.M and J.T.T. work. Computations were performed on UCloud interactive HPC system and

ABACUS2.0 supercomputer, which are managed by the eScience Center at the University of Southern Denmark.

References

[1] Hadron Spectrum collaboration, *A Novel quark-field creation operator construction for hadronic physics in lattice QCD*, *Phys. Rev. D* **80** (2009) 054506 [0905.2160].

[2] P. Boyle, F. Erben, M. Marshall, F. O. Hógáin, A. Portelli and J. T. Tsang, *An exploratory study of heavy-light semileptonic form factors using distillation*, *PoS* **LATTICE2019** (2019) 169 [1912.07563].

[3] N. Cabibbo, *Unitary symmetry and leptonic decays*, *Phys. Rev. Lett.* **10** (1963) 531.

[4] M. Kobayashi and T. Maskawa, *CP Violation in the Renormalizable Theory of Weak Interaction*, *Prog. Theor. Phys.* **49** (1973) 652.

[5] D. London and J. Matias, *B Flavour Anomalies: 2021 Theoretical Status Report*, *Ann. Rev. Nucl. Part. Sci.* **72** (2022) 37 [2110.13270].

[6] C. Morningstar, J. Bulava, J. Foley, K. J. Juge, D. Lenkner, M. Peardon et al., *Improved stochastic estimation of quark propagation with Laplacian Heaviside smearing in lattice QCD*, *Phys. Rev. D* **83** (2011) 114505 [1104.3870].

[7] M. Luscher and S. Schaefer, *Lattice QCD with open boundary conditions and twisted-mass reweighting*, *Comput. Phys. Commun.* **184** (2013) 519 [1206.2809].

[8] M. Bruno et al., *Simulation of QCD with $N_f = 2 + 1$ flavors of non-perturbatively improved Wilson fermions*, *JHEP* **02** (2015) 043 [1411.3982].

[9] A. Gérardin, M. Cè, G. von Hippel, B. Hörz, H. B. Meyer, D. Mohler et al., *The leading hadronic contribution to $(g-2)_\mu$ from lattice QCD with $N_f = 2+1$ flavours of O(a) improved Wilson quarks*, *Phys. Rev. D* **100** (2019) 014510 [1904.03120].

[10] ALPHA collaboration, *Hadron masses and matrix elements from the QCD Schrodinger functional*, *Nucl. Phys. B* **560** (1999) 465 [hep-lat/9903040].